SPACE WEATHER, VOL. 3, S03001, doi:10.1029/2004SW000104, 2005

Interplanetary sources of space weather disturbances in 1997 to 2000

A. V. Dmitriev
Institute of Space Science, National Central University, Chung-Li, Taiwan

Skobeltsyn Institute of Nuclear Physics, Moscow State University, Moscow, Russia

N. B. Crosby
Belgian Institute for Space Aeronomy, Brussels, Belgium

J.-K. Chao
Institute of Space Science, National Central University, Chung-Li, Taiwan

Received 16 July 2004; revised 17 December 2004; accepted 7 January 2005; published 15 March 2005.

[1] Seventy-five disturbed intervals from 1997 through 2000 were analyzed and selected on the basis of space weather effect occurrences such as significant compression of the dayside magnetosphere, strong magnetic storms, ionospheric perturbations, relativistic electron enhancements, and increases in the rate of data failures and radiation doses on board the Mir station. Solar wind disturbances were considered as the main factor influencing the Earth's magnetosphere. We distinguished four geoeffective interplanetary (IP) phenomena: interplanetary coronal mass ejections (ICME), interplanetary forward shocks with compressed region (IS), fast solar wind streams from coronal holes (CH), and corotating interaction regions (CIR) between the CH and relatively slow ambient solar wind. Each selected interval was studied and classified under the IP phenomena that it was a direct consequence of. It was found that IP phenomena "containing" ISs, ICMEs, and CIRs were mostly responsible for geosynchronous magnetopause crossings, strong geomagnetic storms, and intensification of geomagnetically induced currents. The fast solar wind streams from coronal holes controlled mainly geosynchronous relativistic electron enhancements. The rate of data failures and variations of the radiation dose on board the Mir station were related to both IS-ICME and CIR-CH phenomena. Such a relationship was interpreted in terms of (1) decrease of cutoff threshold for solar energetic particles due to the magnetospheric compression and/or ring current intensification on the main phase of geomagnetic storms and (2) intensive relativistic electron precipitation from the outer radiation belt and its contribution to the radiation conditions at low altitudes during recovery phase of recurrent magnetic storms.

Citation: Dmitriev, A. V., N. B. Crosby, and J.-K. Chao (2005), Interplanetary sources of space weather disturbances in 1997 to 2000, *Space Weather*, *3*, S03001, doi:10.1029/2004SW000104.

1. Introduction

[2] It is commonly accepted that interplanetary (IP) phenomena are responsible for such space weather disturbances as enhancements of energetic particle fluxes both in the interplanetary medium and in the magnetosphere, great geomagnetic storms, and strong ionosphere perturbations [*Gosling*, 1993; *Gonzalez et al.*, 1994; *Looper et al.*, 1994; *Tsurutani et al.*, 1995; *Baker et al.*, 1997; *Kamide et al.*, 1998]. Interplanetary coronal mass ejections (ICMEs) and fast/slow solar wind corotating interaction regions (CIRs) corotating with a 27-day period are well known geoeffective IP structures. These IP structures may influence the Earth's magnetosphere when arriving as individual events and/or when a geomagnetic effect from one IP phenomenon is intensified by the disturbance caused by the following IP structure. Those ICMEs with clear field rotations coincident with low temperature and strong magnetic field are known as "magnetic clouds" [*Burlaga et al.*, 1981]. An interaction between ICMEs or between an ICME and a CIR leads to the compression of the magnetic cloud and intensifies the magnetic field at the interaction region of the cloud [*Burlaga et al.*, 1987; *Bothmer and Schwenn*, 1995; *Dal Lago et al.*, 2001]. This intensification of the magnetic field with southward orientation is closely related to the occurrence of intense geomagnetic storms.

[3] The ICME or ejecta as described by *Burlaga et al.* [2001] are transient, noncorotating solar wind flows that may have either an ordered internal magnetic field structure of a flux rope (magnetic clouds) or a disordered magnetic field (complex ejecta), which is due to complex internal field structure or to interaction of the magnetic cloud with other IP structures. The main signatures of the ejecta indicated in [*Burlaga et al.*, 1981; *Gosling*, 1990] are the following: enhanced interplanetary magnetic field

(IMF) strength, low variance of IMF, relatively low ion temperature, high relative abundance of He, and counterstreaming electrons. The ejecta may propagate either with velocities much higher than the ambient solar wind (fast ejecta) or with velocities of about the strength as those of the downstream solar wind speed (slow ejecta). In front of the fast ejecta an interplanetary shock and a sheath region are formed. The sheath region is compressed and therefore characterized by the disturbed solar wind having a relatively high density and high amplitude of the IMF intensified by the compression. The sheath region has sometimes a much larger size than the ejecta driving it. Because of this the Earth's magnetosphere may be intersected only by the disturbed solar wind from the sheath, but the ejecta itself may be missed [*Borrini et al.*, 1982; *Sheeley et al.*, 1985].

[4] The corotation interaction region (CIR) is formed by the interaction of the fast solar wind expanding from solar coronal holes with ambient slow solar wind streams originating from the border of coronal holes or from the heliospheric current sheet [e.g., *Zhang et al.*, 2003a; *Tsurutani et al.*, 1995]. The fast solar wind is characterized by strong Alfven waves causing a high variability of the IMF orientation. The density and velocity of the fast solar wind can also vary significantly. Such variability is a source of long duration and very intense substorm activity in the magnetosphere [*Wilcox and Ness*, 1965; *Tsurutani and Gonzalez*, 1987]. The interaction of the fast and slow solar wind leads to compression of the plasma and magnetic field inside the CIR. As a result the density (D) and IMF strength (B) in the CIR are characterized by very high values similar to those found in the sheath region ($D \sim 20$ cm^{-3} and $B \sim \pm 20$ nT). The magnetic field direction is disordered and highly variable. Usually the CIR is well developed far beyond the Earth's orbit (at $2 \sim 4$ AU) and the interplanetary forward shock is not formed in most CIRs observed near the Earth [*Gosling et al.*, 1976]. However, in some cases the orientation of the IMF in the heliospheric current sheet promotes the interplanetary shock formation in the Earth's orbit at 1 AU [*Chao et al.*, 1986]. The interplanetary shock can also appear as a result of the interaction between the ICMEs or between the CIR and the ICME [*Borrini et al.*, 1982].

[5] Numerous studies have been devoted to identification of interplanetary disturbances and their geoeffectiveness during the rising phase and maximum of the current solar cycle. A catalogue of the solar energetic particle events and corresponding ICMEs in 1997–2001 was created by *Cane et al.* [2002]. *Cane and Richardson* [2003] published a list of interplanetary ejecta detected near the Earth in 1996 to 2002. Analysis of the IP sources of major geomagnetic storms in 1996 to 2000 [*Zhang et al.*, 2003b] showed that 26 of 27 storms with $Dst < -100$ nT are associated with ICMEs and only one storm is caused by a CIR. Note that a similar result was obtained by *Bothmer and Schwenn* [1995] for strong geomagnetic storms with $Kp \geq 8$ during the years 1966–1990, that is, for two solar cycles.

[6] Classification of the geoeffective IP phenomena and their geomagnetic consequences during the rising phase of the current solar cycle was performed by *Huttunen et al.* [2002]. They investigated the magnetic clouds, interplanetary shocks, sheath regions and CIRs as solar wind drivers of about 100 magnetic storms occurring from 1996 to 1999. The authors found a difference in behavior of the storms in *Kp* and *Dst* indices during the different types of solar wind drivers. Namely more *Kp* storms were associated with the interplanetary shocks and sheath regions, but the ejecta generated more *Dst* storms. It was found that the strongest geomagnetic storms ($Dst \leq -200$ nT, or $Kp \geq 8$), are associated either with fast ejecta accompanied by a forward shock or with a sheath region. However, in that study the IP phenomena were considered as separate structures without the possible interaction of one phenomenon with another, so that the cumulative effect of their possible consequences on the magnetosphere was not taken into account.

[7] The work that is presented here considers the interaction of IP phenomena and is devoted to alternative scenarios. 75 space weather intervals from 1997 to 2000 (http://dec1.npi.msu.su/~dalex/intas/SWITDB/) are analyzed. The intervals are selected using information about geomagnetic disturbances, enhancements of trapped radiation, radiation effects on board the Mir station, and increases of geomagnetically induced current (GIC) activity. As shown in [*Dmitriev and Crosby*, 2003] only one third of the intervals are strictly associated with magnetic clouds that pass the Earth. The solar wind drivers of the remaining intervals require further detailed consideration. The method in which the disturbed space weather intervals were selected is described in section 2. Section 3 introduces the interplanetary structures, which drive the space weather effects in the disturbed intervals. The various IP sequence scenarios are defined in section 4. Section 5 concerns how the space weather effects and especially radiation effects depend on the IP sequence. In section 6 the results are discussed and a summary is given.

2. Space Weather Disturbances

[8] Disturbed space weather intervals from 1997 to 2000 are listed in the Space Weather Interval Table (SWIT) catalogue, which is available on the Web site (http://dec1.npi.msu.su/~dalex/intas/SWITDB/). The 75 SWIT intervals and their characteristics are listed in Table 1. An interval consists of consecutive days during which at least one of the following space weather effects (with a defined threshold) is encountered: geosynchronous magnetopause crossings (GMC), geomagnetic disturbances in *Dst*, *Kp*, *Ap*, and *PC* indices, enhancements of relativistic electron fluxes at geosynchronous orbit, radiation doses and data failures in the equipment on board the Mir station, and increases of the *DB* index. The daily DB index is calculated on the base of 1-min time derivatives of the horizontal magnetic field, which is measured by the IMAGE magnetometer network [*Lühr*, 1994]. The index is

Table 1. SWIT Intervals and Related IP Phenomena[a]

	Year	Start Month	Start Day	End Month	End Day	IS	ICME	CIR	CH	Class	XF	SEP	GLE	FE	GMC	*Dst*	*Kp*	*Ap*	*PC*	GREE	*D*1	*D*2	*Z*1	*Z*2	*DB*
1	1997	1	10	1	15	1	1	1	1	MIX	·	·	·	·	+	·	·	+	·	+	+	·	–	–	·
2	1997	1	28	2	2	0	0	1	1	CHS	·	·	·	·	·	·	·	+	·	+	·	+	–	–	+
3	1997	2	5	2	7	1	1	0	0	ITS	·	·	·	·	·	·	·	·	·	+	·	+	–	–	·
4	1997	2	8	2	17	1	3	1	1	MIX	·	+	·	·	+	·	·	+	·	+	+	+	–	–	+
5	1997	2	27	3	5	1	1	1	1	MIX	·	·	·	·	·	·	+	+	·	+	·	+	–	–	·
6	1997	3	11	3	12	0	0	1	1	CHS	·	·	·	·	·	·	·	·	·	·	+	+	–	–	·
7	1997	4	10	4	11	1	1	1	1	MIX	·	·	·	+	·	·	+	+	·	·	·	·	–	–	+
8	1997	5	15	5	15	1	1	1	1	MIX	·	·	·	·	+	+	+	+	+	+	·	·	–	–	+
9	1997	5	26	5	27	1	1	0	0	ITS	·	·	·	·	·	·	·	+	·	·	·	·	–	–	+
10	1997	6	9	6	9	1	1	0	0	ITS	·	·	·	·	·	·	·	+	·	·	·	·	–	–	+
11	1997	9	3	9	14	1	1	1	1	MIX	·	·	·	·	+	·	·	+	·	+	·	·	–	–	·
12	1997	10	10	10	11	1	1	0	0	ITS	·	·	·	·	·	+	·	+	·	+	·	·	–	–	+
13	1997	11	4	11	5	0	0	0	0	–	+	+	·	·	·	·	·	·	·	·	+	+	–	–	·
14	1997	11	6	11	8	1	1	0	0	ITS	+	+	+	·	+	+	+	+	·	·	+	+	–	–	+
15	1997	11	22	11	30	1	1	1	1	MIX	·	+	·	·	+	+	+	+	·	+	+	+	–	–	+
16	1998	3	10	3	14	0	0	1	1	CHS	·		·	·	+	+	+	+	+	+	·	–	–	–	+
17	1998	4	23	4	30	0	0	1	1	CHS	+	+	·	·	·	·	·	+	·	+	·	–	–	–	·
18	1998	5	1	5	6	2	2	0	0	ITS	+	+	+	+	+	+	+	+	+	+	+	–	–	–	+
19	1998	5	6	5	15	0	1	1	1	MIX	+	+	+	·	·	·	·	+		+	+	–	–	–	·
20	1998	6	6	6	10	0	0	1	1	CHS	·	·	·	·	·	·	·	·	·	+	+	+	–	–	·
21	1998	6	26	6	27	1	1	0	0	ITS	·	–	·	·	·	+	·	+	·	·	·	·	+	·	+
22	1998	7	4	7	6	1	1	1	0	MIX	·	–	·	+	·	·	·	·	·	·	+	+	–	–	·
23	1998	7	16	7	18	0	0	1	1	CHS	·	–	·	·	+	·	·	+	·	+	·	·	+	+	+
24	1998	7	23	7	28	0	0	1	1	CHS	·	–	·	·	·	·	·	+	·	+	+	+	+	+	·
25	1998	8	6	8	7	0	1	1	1	MIX	·	–	·	·	+	+	+	+	+	·	+	–	–	–	·
26	1998	8	19	8	20	1	1	0	0	ITS	+	–	·	·	·	·	·	·	+	·	+	+	–	–	·
27	1998	8	21	8	22	0	0	1	1	CHS	+	–	·	+	·	·	·	·	+	·	+	–	–	–	·
28	1998	8	25	9	5	1	1	0	1	MIX	+	+	+	+	+	+	+	+	+	+	+	+	+	+	+
29	1998	9	24	9	30	1	1	0	1	MIX	·	+	·	+	+	+	+	+	+	+	+	+	+	+	+
30	1998	10	1	10	7	0	0	1	1	CHS	·	·	–	·	·	·	·	+	·	+	·	+	+	·	·
31	1998	10	7	10	10	0	0	1	1	CHS	·	·	–	·	·	·	·	+	·	+	·	·	+	·	·
32	1998	10	19	10	23	1	1	1	1	MIX	·	–	·	·	+	+	·	+	·	+	+	+	+	+	+
33	1998	10	23	10	25	1	1	0	1	MIX	·	·	·	+	·	·	·	·	·	+	·	·	+	+	·
34	1998	11	5	11	9	2	2	0	0	ITS	+	+	·	+	+	+	+	+	+	·	·	·	–	–	+
35	1998	11	13	11	20	1	1	1	1	MIX	·	+	·	·	·	+	·	+	+	+	+	·	+	+	+
36	1999	1	13	1	14	1	1	1	1	MIX	·	–	·	·	·	+	+	+	+	·	·	·	·	·	·
37	1999	2	18	2	19	1	1	1	0	MIX	·	–	·	+	+	+	+	+	+	·	·	·	+	·	+
38	1999	3	1	3	2	1	1	1	1	MIX	·	·	·	·	·	·	·	+	·	·	·	+	·	·	+
39	1999	3	10	3	10	1	1	0	0	ITS	·	·	·	·	+	·	·	+	·	–	·	·	·	·	+
40	1999	3	29	3	30	0	0	1	1	CHS	·	·	·	·	+	·	·	+	·	–	·	·	·	·	·
41	1999	4	16	4	17	1	1	0	0	ITS	·	·	·	·	+	+	+	+	·	·	+	·	–	–	+
42	1999	4	29	5	4	0	0	1	1	CHS	·	·	·	·	·	·	·	+	·	+	+	·	·	·	·
43	1999	5	5	5	12	0	0	1	1	CHS	·	+	·	+	·	·	·	·	·	+	+	+	–	–	·
44	1999	6	26	6	28	2	2	0	0	ITS	·	+	·	+	+	·	·	+	·	·	+	·	+	+	+
45	1999	7	30	7	31	1	1	0	0	ITS	·	–	·	·	+	·	+	+	·	·	–	–	·	·	·
46	1999	8	19	8	24	1	1	1	1	MIX	·	+	·	+	·	·	·	+	+	+	–	–	·	·	+
47	1999	8	28	9	6	0	0	1	1	CHS	+	·	·	·	+	·	·	+	·	+	–	–	+	+	·
48	1999	9	12	9	21	1	1	1	1	MIX	·	+	·	·	·	·	·	+	·	+	–	–	·	·	+
49	1999	9	21	9	23	1	1	0	0	ITS	·	+	·	·	+	+	+	+	·	·	–	–	·	·	·
50	1999	9	27	10	3	0	0	1	1	CHS	·	·	·	·	·	·	·	+	·	+	–	–	·	·	+
51	1999	10	10	10	21	0	0	1	1	CHS	·	·	·	·	·	·	·	+	·	+	–	–	+	·	+
52	1999	10	21	10	28	1	1	0	1	MIX	·	·	·	·	+	+	·	+	·	+	–	–	+	+	+
53	1999	11	7	11	12	0	0	1	1	CHS	·	+	·	·	·	·	·	+	·	+	–	–	+	+	+
54	2000	1	1	1	6	0	0	1	1	CHS	·	+	·	·	·	·	·	+	·	+	–	–	+	+	+
55	2000	1	11	1	12	0	0	1	1	CHS	·	+	·	·	·	·	·	+	+	·	–	–	+	+	·
56	2000	1	22	1	23	1	1	0	0	ITS	·	+	·	·	·	·	·	+	·	·	–	–	+	+	+
57	2000	1	27	2	3	0	0	1	1	CHS	·	+	·	·	+	·	·	+	·	+	–	–	·	·	+
58	2000	2	5	2	10	0	0	1	1	CHS	+	+	·	·	·	·	·	+	·	+	–	–	+	+	·
59	2000	2	11	2	12	2	2	0	0	ITS	·	+	·	+	+	+	+	+	·	·	–	–	·	·	+
60	2000	2	23	2	29	0	0	1	1	CHS	·	+	·	+	·	·	·	+	·	+	–	–	+	+	·
61	2000	4	6	4	12	1	1	0	1	MIX	·	+	·	·	+	+	+	+	·	+	–	–	–	–	+
62	2000	5	17	5	18	1	1	1	1	MIX	·	+	·	·	·	·	·	+	·	·	·	·	+	+	+
63	2000	5	23	5	28	2	2	0	0	ITS	·	+	·	·	+	+	+	+	·	+	–	–	+	+	+
64	2000	6	7	6	9	1	1	0	0	ITS	+	+	·	+	+	·	+	+	+	+	–	–	–	–	+
65	2000	7	11	7	13	2	2	0	0	ITS	+	+	·	+	+	·	+	+	·	·	–	–	–	–	+
66	2000	7	14	7	17	3	3	0	0	ITS	+	+	+	+	+	+	+	+	+	+	–	–	–	–	+
67	2000	8	11	8	12	2	2	0	0	ITS	·	+	·	·	+	+	+	+	+	+	–	–	–	–	+
68	2000	9	17	9	24	1	1	0	1	MIX	·	+	·	+	+	+	·	+	+	+	–	–	–	–	+

Table 1. (continued)

	Year	Start Month	Start Day	End Month	End Day	IS	ICME	CIR	CH	Class	XF	SEP	GLE	FE	GMC	*Dst*	*Kp*	*Ap*	*PC*	GREE	*D*1	*D*2	*Z*1	*Z*2	*DB*
69	2000	10	2	10	4	1	1	0	0	ITS	·	+	·	+	·	+	+	+	·	·	–	–	–	–	+
70	2000	10	5	10	6	1	1	0	0	ITS	·	+	·	·	+	+	+	+	·	·	–	–	–	–	+
71	2000	10	13	10	14	1	1	0	0	ITS	·	+	·	·	·	+	·	+	·	·	–	–	–	–	+
72	2000	10	26	10	29	1	1	0	0	ITS	·	+	·	+	·	+	·	+	·	+	–	–	–	–	+
73	2000	11	6	11	9	1	1	0	0	ITS	·	·	·	+	+	+	+	+	+	+	–	–	–	–	+
74	2000	11	8	11	18	2	2	1	1	MIX	·	+	·	+	+	+	·	+	+	+	–	–	–	–	+
75	2000	11	26	11	29	1	1	0	0	ITS	+	+	·	+	+	+	+	+	+	·	–	–	–	–	+

[a]A plus indicates that the parameter is disturbed. A minus indicates that no data are available for the parameter. A dot means that there is no disturbance of the parameter.

considered as a relevant indicator of geomagnetically induced current (GIC) activity caused by disturbances in the high-latitude ionosphere.

[9] The GMCs are identified using data from the geosynchronous satellites GOES and LANL [*Suvorova et al.*, 2005]. Geosynchronous relativistic electron enhancements (GREEs) are determined when daily maximal fluxes of >2 MeV electrons measured by GOES 8 at geosynchronous orbit are higher than 1500 $(cm^2\ s\ sr)^{-1}$ [*Dmitriev and Chao*, 2003]. Geomagnetic disturbances are characterized by different geomagnetic indices. Days with strong magnetic storms are identified when the daily minimal 1-hour *Dst* variation is less than −100 nT. Days with disturbed auroral activity are determined when the daily averaged *Ap* index is more than 20 or when the maximal 3-hour *Kp* index is higher than 6.5 [*Bothmer et al.*, 2002]. Daily maximal 1-hour *PC* index higher than 10 indicates days with disturbances in the polar cap [*Troshichev et al.*, 1988; *Dmitriev and Chao*, 2003].

[10] Our definition of space weather damage is characterized by the number of operational errors in the scientific equipment and the radiation dose measured on board the Mir orbital station. The disturbances in the operation of scientific equipment are determined in [*Dmitriev et al.*, 2002] as increases of the daily probability of errors in the data from the gas discharge counter (*Z*1) or in the data from the scintillation detector NaI (*Z*2) that is more than one root mean square deviation (RMSD) of their average values, that is, >0.051 and >0.061, respectively, in logarithmic scale. The radiation doses *D*1 and *D*2 were measured on board the Mir station [*Panasyuk et al.*, 1998; *Tverskaya et al.*, 2004] under equivalent aluminum shields of 4.5 g/cm^2 and 2 g/cm^2. Therefore the doses are produced by protons with energies E > 70 MeV and E > 40 MeV, respectively, and by electrons with energies E > 8.5 MeV and E > 4 MeV, respectively. Figure 1 represents the logarithmic values of the doses *D*1 and *D*2 in arbitrary units. Disturbed days for

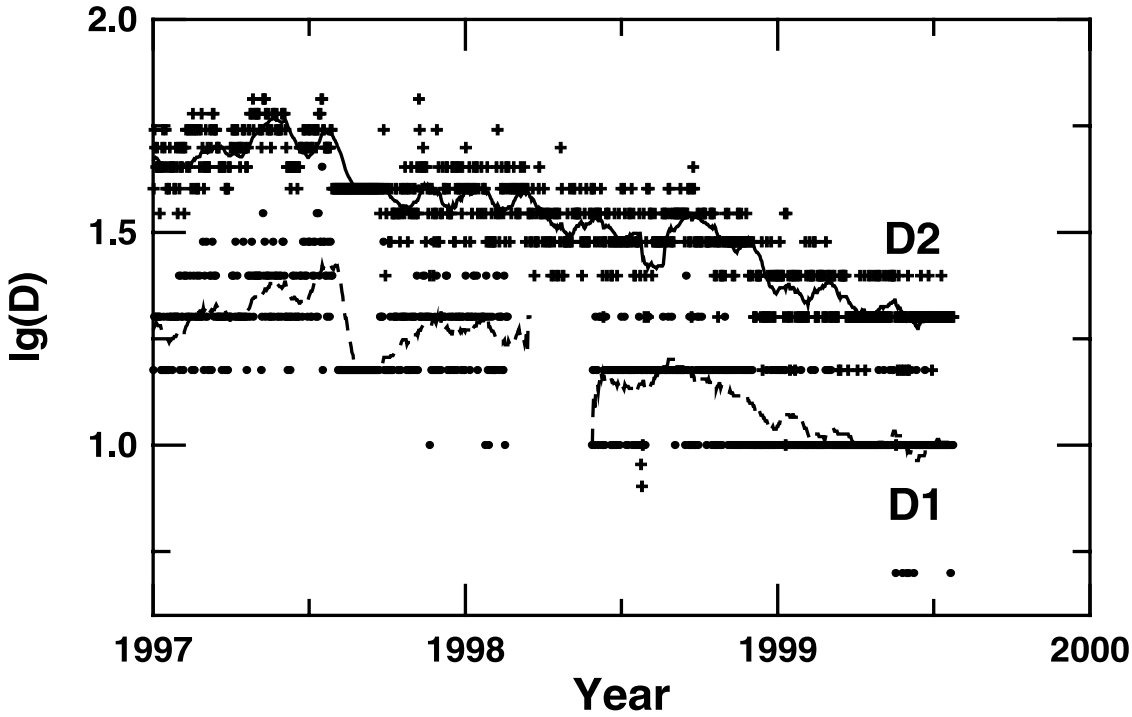

Figure 1. Variations of the daily averaged logarithms of radiation doses *D*1 (circles) and *D*2 (crosses) on board Mir station in 1997 to 2000. Running 27-day averaged logarithmic values of *D*1 and *D*2 are plotted by dashed and solid lines, respectively. See details in the text.

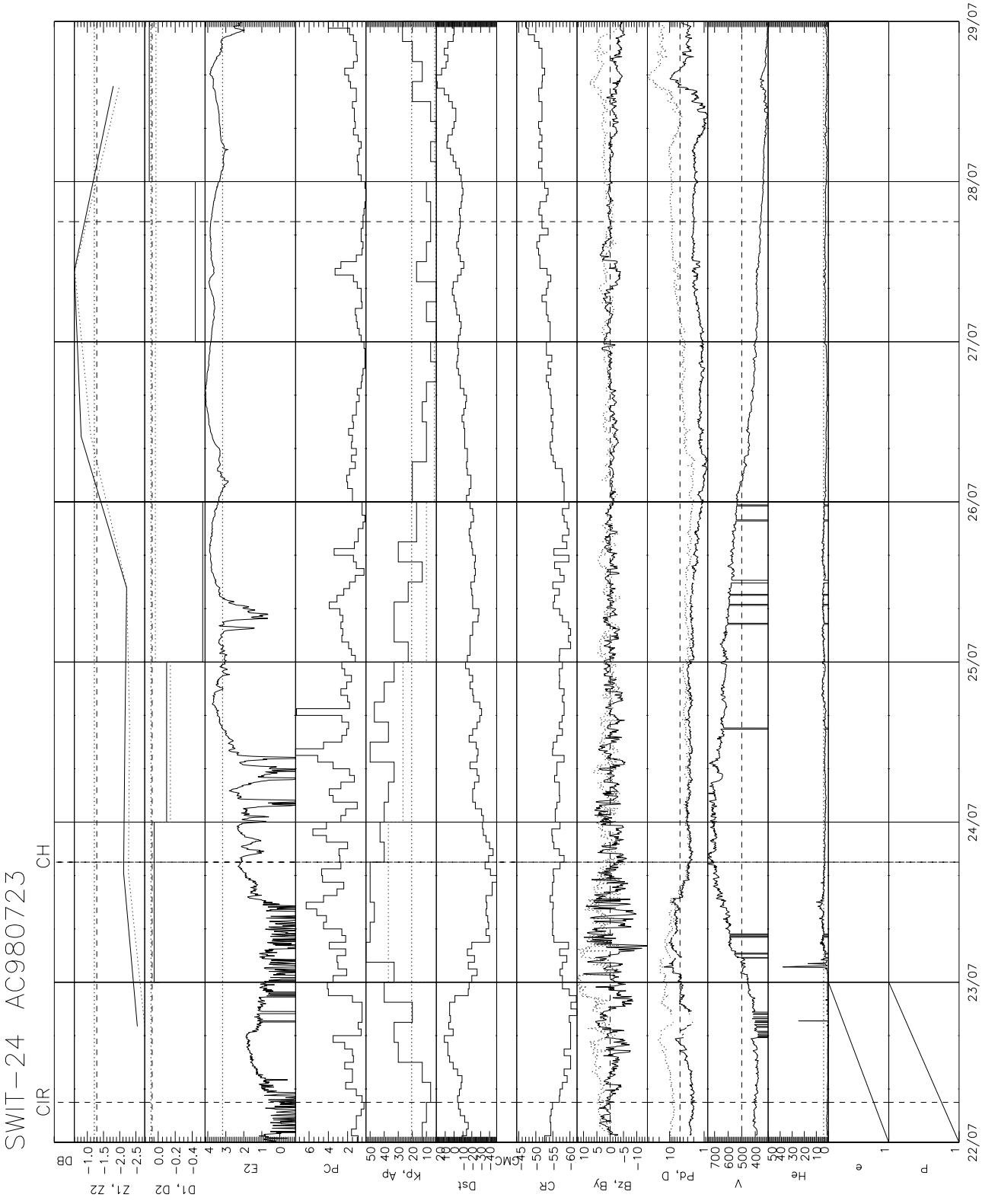
SWIT–24 AC980723
CIR
CH
DB
Z1, Z2
D1, D2
E2
PC
Kp, Ap
Dst
SMC
CR
Bz, By
Pd, D
V
He
e
p
22/07
23/07
24/07
25/07
26/07
27/07
28/07
29/07

Figure 2

the parameters $D1$ and $D2$ are determined when the variation of the radiation doses relative to their running 27-day averaged value is larger than one RMSD, that is, >0.071 and >0.085, respectively, in logarithmic scale.

[11] Radiation effects in the magnetosphere and ionospheric disturbances can be caused by enhancements of the solar X-ray radiation and solar energetic particles (SEP) [e.g., *Poppe*, 2000; *Hanslmeier*, 2002]. In the SWIT catalogue we indicate very powerful solar X-ray flares of type >M8 (parameter *XF*) obtained by GOES monitoring measurements of solar X-ray emission (ftp://solar.sec.noaa.gov/pub/indices/events). The other parameters describing the solar and heliospheric perturbations are SEP fluxes with energies E >10 MeV (*SEP*) detected by the GOES geosynchronous satellites (http://sec.noaa.gov/ftpdir/indices/SPE.txt). Note that the fluxes of high-energy protons observed at geosynchronous orbit are very close to that observed in the interplanetary medium [*Cohen et al.*, 2001]. We define the parameter *SEP* as being disturbed when the fluxes of protons with corresponding energies exceed the threshold value of 10^{-2} $(cm^3\ s\ sr)^{-1}$. We also use variations of cosmic rays as an indirect indicator of very powerful solar and interplanetary disturbances [*Gosling*, 1993; *Cane*, 2000; *Kudela et al.*, 2000; *Tylka*, 2001]. Intensive fluxes of high energy and relativistic nucleons are generated in solar X-ray flares or on strong foreshocks of interplanetary transients. Forbush decreases are caused by large-scale interplanetary disturbances such as ICMEs and can also be caused by CIRs. The SWIT catalogue includes ground level enhancement (GLE) events with cosmic ray amplitude variation >3% (http://pgi.kolasc.net.ru/CosmicRay/), and large Forbush decreases (*FE*) of cosmic rays (http://helios.izmiran.rssi.ru/cosray/events.htm).

3. Identification of IP Structures

[12] We study the interplanetary disturbance as a sequence (IP sequence) of well-known IP phenomena. Namely there are: (1) interplanetary transient or ICME; (2) interplanetary shock and sheath region (IS), which can be formed ahead the ICME; (3) fast solar wind stream (CH) originating from solar coronal holes; (4) corotating interaction region (CIR), which is always formed ahead of the fast solar wind interacting with the ambient slow and dense plasma streams.

[13] We identify an ICME as a structure with gradually changing IMF and plasma properties that is characterized by helium abundance. Large Forbush decreases are used as an indirect indication of the ICME occurrence. We also use information about near-Earth space crossings by ICMEs, which is available on the Web site (http://lepmfi.gsfc.nasa.gov/mfi/mag_cloud_pub1.html#table) and presented in the catalogue by *Cane and Richardson* [2003]. Note that the latter catalogue also provides information about the ICME-associated forward shocks and sheath regions. Corotating fast streams from coronal holes are identified using time profiles of the solar wind velocity and IMF B_x component during consequent Bartles rotations and maps of coronal holes observed on the Sun (ftp://ftp.noao.edu/kpvt/daily/lowres/). The IS and CIR are determined as regions with strong compression of the interplanetary plasma and IMF ahead of the ICME and CH respectively. It is rather difficult to distinguish the IS and CIR when the ICME itself is not registered. In this case a compressed IP structure is attributed to the CIR.

[14] The strength of the IS and CIR can be increased significantly because of the interaction between the CH and ICME so that the solar wind pressure and IMF strength (including southward component) may achieve the values of a few tens of nPa and nT respectively. Such conditions provide extremely strong energy input in the magnetosphere. The way this energy is redistributed in the magnetosphere and ionosphere is mainly controlled by the orientation of the IMF [*Akasofu*, 1981].

[15] Examples of the IP driver identification for the SWIT intervals are presented in Figures 2 and 3. The experimental information about the solar wind plasma and IMF is provided by the Wind, SOHO CELIAS/MTOF (http://umtof.umd.edu/pm/) and ACE (http://www.srl.caltech.edu/ACE/) satellites. Measurements of interplanetary fluxes of the electrons and protons are performed by the SOHO satellite. The data on the interplanetary conditions

Figure 2. IP drivers and space weather effects on 22–28 July 1998 (SWIT-24 interval). Top to bottom: bar indicator of the *DB* index enhancements; logarithmic rates of the data failures $Z1$ and $Z2$ on board the Mir station (solid and dashed curves, respectively); logarithmic deviations from the running 27-daily average of radiation doses $D1$ and $D2$ on board the Mir station (solid and dashed histograms, respectively); >2 MeV electron flux (in log scale) measured by GOES 8; *PC* index of the magnetic activity in the South Polar region; *Kp* and *Ap* (daily) indices of geomagnetic activity (solid and dashed histograms, respectively); *Dst* index of the geomagnetic storm; bar indicator of the GMC; hourly averaged variation (in 0.1%) of 10 GeV cosmic rays; IMF B_z and B_y (nT) components in GSM (solid and dashed curves, respectively); solar wind dynamic pressure *Pd* (nPa) and density D (cm^{-3}) indicated by solid and dashed curves, respectively; solar wind velocity V (km/s); helium/proton ratio *He* (%); interplanetary fluxes of electrons in the energy channels 0.5–1.8, 1.8–4.4, and >4.4 MeV; and interplanetary fluxes of protons in the energy channels 0.54–1.37, 1.37–4.01, 4.01–6.1, 6.1–16.4, 16.4–33., and >33. MeV. Horizontal short-dashed and long-dashed lines indicate the thresholds for disturbances of the corresponding parameters. Vertical dashed lines indicate approximate boundaries of the IP structures: corotating interaction region (CIR) and fast solar wind from the coronal holes (CH).

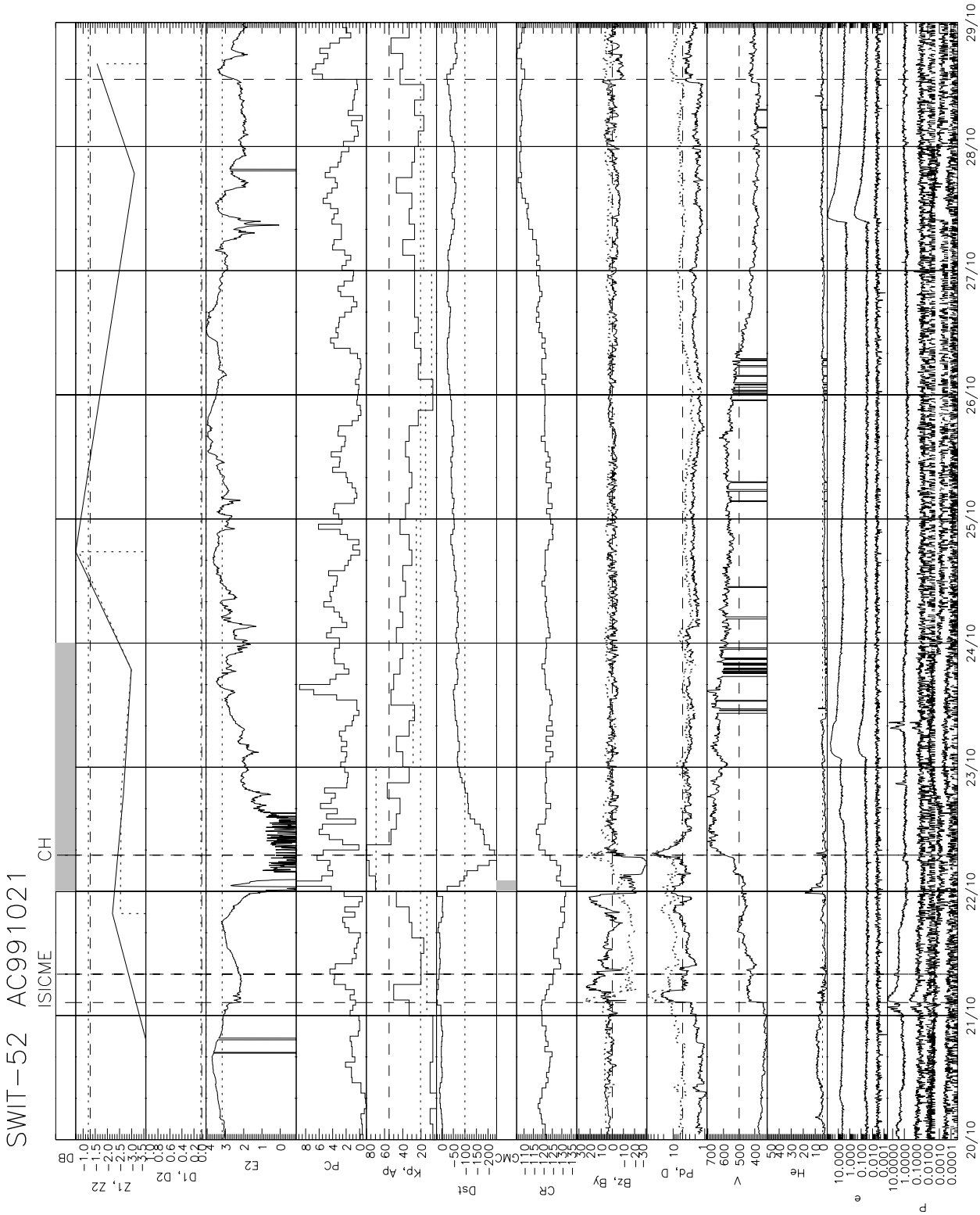
SWIT–52 AC991021
ISICME
CH
DB
Z1, Z2
D1, D2
E2
Pc
Kp, Ap
Dst
GMC
CR
Bz, By
Pd, D
V
He
e
P
20/10
21/10
22/10
23/10
24/10
25/10
26/10
27/10
28/10
29/10

Figure 3

is obtained from the ISTP database (http://cdaweb.gsfc.nasa.gov/cdaweb/istp_public/).

3.1. Example 1: SWIT-24

[16] Figure 2 illustrates the SWIT-24 interval. From 22 to 27 July 1998 we observe a substantial increase of the data failure rates ($Z1$, $Z2$) and radiation doses ($D1$, $D2$) on board the Mir station and GREEs ($E2$), as well as an increase of the geomagnetic activity in the polar region (PC index) and high-latitude ionosphere and magnetosphere (Kp and Ap indices). These phenomena are accompanied by a weak geomagnetic storm with $Dst > -50$ nT and very small cosmic ray variations. At the same time conditions in the interplanetary medium are highly disturbed. The ACE satellite measures a long-lasting enhancement of the solar wind dynamic pressure up to 10 nPa from 22 to 23 July and the IMF B_z has high amplitude (up to -13 nT) fast variations. The solar wind velocity increases from $\sim$400 km/s on July 22 to $\sim$750 km/s on 23 and 24 July and then gradually decreases to its initial value. We attribute the compressed region with highly varying IMF (from $\sim$6 UT on 22 July to $\sim$18 UT on 23 July) to the CIR, which precedes the fast solar wind from the coronal hole observed during more than three days after $\sim$18 UT on 23 July. The SWIT-24 interval is a typical example of space weather disturbances associated with a CIR-CH sequence: a corotating interaction region and fast solar wind streams originating from a solar coronal hole. Note that during this interval there are no interplanetary ejecta indicated in the ICME catalogues.

3.2. Example 2: SWIT-52

[17] Another kind of IP sequence in the SWIT-52 interval is presented in Figure 3. An interplanetary transient interacts with fast solar wind streams originating from a coronal hole. The IP structure observed by the ACE satellite from $\sim$2 UT on 21 October 1999 to $\sim$10 UT on 22 October 1999 demonstrates practically all properties of a magnetic cloud: gradual rotation of the magnetic field, low proton temperature and density, high He contribution and magnetic field strength. The magnetic cloud is preceded by a forward shock and compressed sheath region at $\sim$2 UT on 21 October. The shock accelerates the protons in the interplanetary medium and their flux increases when the shock approaches the Earth. The back region of the magnetic cloud (since $\sim$4 UT) strongly interacts with fast solar wind streams expanding from the coronal hole. The interaction ends at $\sim$10 UT on 22 October when the IMF B_x component turns in an anti-Sun direction and the solar wind speed reaches 700 km/s. Because of this interaction the magnitude of the southward IMF B_z is intensified from -20 nT to -30 nT. Such intensification causes a great geomagnetic storm on 22 October 1999 when the maximal Dst variation exceeds -200 nT, $Kp = 8$, daily $Ap \sim 70$ and maximal $PC \sim 9$.

[18] The geosynchronous magnetopause crossing is observed after midnight on 22 October. Its short duration is explained by the fact that only data from LANL 1997 are available for the dayside magnetosphere. Actually the duration of the GMC interval on 22 October, when the magnetopause enters inside the geosynchronous orbit, should be much larger. It is important to note that the geosynchronous relativistic electron flux on the night side (local midnight for the GOES 8 spacecraft corresponds to 5 UT) diminishes just at the beginning of the geomagnetic storm. A sharp and significant increase of the electron flux at $\sim$2 UT (more than 3 orders of magnitude) is observed and coincides with increase of the PC index while the Kp index does not reach maximum until some hours later. Moreover the relativistic electron flux becomes very weak when the Kp index has maximal values from 3 UT to 9 UT on 22 October.

[19] The other interesting particularity of the SWIT-52 interval is that the DB index is enhanced on both the stormtime day (21 October) and on the next day (22 October) when the geomagnetic activity becomes much weaker and is supported only by Alfven waves within the fast solar wind streams. During the rest of the days of the SWIT-52 interval when the CH structure intersects the Earth (23–26 October) the behavior of the geosyncronous relativistic electron fluxes ($E2$) and the rates of data failures on board the Mir station ($Z1$ and $Z2$) resemble the SWIT-24 interval: they gradually increase and exceed their thresholds for disturbance on the second or third day after the maximum of the geomagnetic storm.

4. Geoeffective IP Disturbances

[20] Using the results described in section 3 we can apply Table 1 for a statistical analysis. As can be seen from Table 1 all of the four above considered IP phenomena (IS, ICME, CIR or CH) are geoeffective, in other words they can contribute to space weather disturbances. For each given SWIT interval, Table 1 contains the number of different IP structures observed within the interval and indicators of disturbance for different space weather parameters. The parameter in Table 1 is considered disturbed (indicated by a plus) if its value exceeds the corresponding threshold for the disturbance indicated in section 2. A minus indicates that no data are available for a parameter. A dot means that there is no disturbance of the parameter. Our statistical analysis is based on the comparison between the IP sequences responsible for disturbed space weather conditions in the SWIT intervals.

[21] The total number (NN) of IP phenomena and percentage of the different kinds of IP phenomena (in parentheses) revealed in the SWIT catalogue are presented in Table 2 (second column). The number of SWIT intervals that are associated with an IP phenomenon and their

Figure 3. Same as Figure 2 but for SWIT-52 interval on 20–28 October 1999. Vertical dashed lines indicate approximate boundaries of the IP structures: interplanetary sheath (IS), interplanetary transient (ICME), and fast solar wind from the coronal holes (CH).

Table 2. Number of Different IP Phenomena in the SWIT Intervals[a]

IP Phenomenon	N	N_{SWIT}
IS	60 (29)	50 (68)
ICME	64 (30)	52 (70)
CIR	41 (20)	41 (55)
CH	45 (21)	45 (61)

[a]Numbers in parentheses indicate percent.

percentage (in parentheses) are indicated in the third column of Table 2. It should be noted that the number of the SWIT events associated with solar wind disturbances is 74. Radiation effects in SWIT-13 interval were caused by a SEP event from a X2.1 class solar flare at 0552 UT on 4 November 1997 [see *Cane et al.*, 2002]. It is seen in Table 2 that the ICME phenomenon has the highest association with the SWIT intervals (70%). However, associations of the CH and CIR phenomena to the SWIT intervals are also significant (~60%). As this value is comparable with the ICME contribution a consideration of the CH and CIR phenomena as possible sources of space weather disturbances is required.

[22] We now consider the geoeffective IP conditions as a sequence (IP sequence) of the above described phenomena: IS + IT + IR + CH. Such consideration permits taking into account the possible interaction between different IP structures and identification of complex events. Obviously different parts of this sequence can be absent in different space weather events. Therefore we introduce a classification of IP structures on the basis of different realizations of the IP sequence. Table 3 presents possible scenarios of the geoeffective IP situation and its relation to different classes of the IP sequence. We distinguish between three main classes: (1) ITS class associated with interplanetary transients, (2) CHS class associated with fast solar wind from coronal holes, and (3) complex events (MIX). The class of interplanetary transients, ITS, includes IP events where the space weather disturbances are caused by single or multiple ICME and/or IS structures. The CHS class includes fast solar wind originating from coronal holes (CH) together with corotating interaction regions (CIR). The MIX class combines all complex events where interplanetary transients interact with fast solar winds from coronal holes forming strong IS and/or CIR phenomena. Note that for the MIX class events the fast solar wind from the coronal holes can influence the space weather situation substantially later in the time sequence (at least 12 hours). In this case there is no interaction between the ICME and CH structures. However, a CH phenomenon can contribute to a space weather disturbance producing a secondary intensification of the geomagnetic storm as well as long-lasting geomagnetic perturbations in the auroral region.

[23] Table 3 shows that different classes of the IP sequence are represented in the SWIT catalogue with practically equal percentages: 36% of the ITS, 30% of the CHS and 34% of the MIX events. Hence about one third of space weather disturbances is caused by only ICMEs. Fast solar wind streams from the solar coronal holes cause also 30% of the space weather disturbances and another third is very complicated IP situations that originate from the interaction of occasional solar eruptive events with quasi-stationary corotating solar wind structures.

Table 3. Number of SWIT Events for Different Classes of the IP Sequence

IP Class	Percent	N	IS	ICME	CIR	CH
ITS	36	27	X	X		
CHS	30	22			X	X
MIX		15	X	X	X	X
		2	X	X	X	
		2		X	X	X
		6	X	X		X
Total for MIX	34	25				

5. Space Weather Effects

[24] Using the above described classification of the IP disturbances we can now investigate how space weather effects from the SWIT intervals depend on the IP sequence. For this purpose we calculate the number of cases N_{ef} when a given space weather effect is associated with a given class of IP sequence. The percentage (P_{ef}) of IP events from a given class that cause the given space weather effect is determined as

$$P_{ef} = 100\% \, N_{ef} \Big/ N_{IP}, \quad (1)$$

where N_{IP} is the total number of IP events from the given class for the time period when the given space weather effect is observed. The results of the P_{ef} calculation are presented in Table 4.

[25] Consideration of the different IP sequences observed in the SWIT intervals in connection with space weather effects (Table 4) leads to the following conclusions:

[26] 1. Geosynchronous magnetopause crossings, GMC, are observed in 49% of the SWIT intervals. The ITS and MIX classes of the IP sequence contribute mostly to the observed GMCs. It is very interesting that GMCs are also caused by CIR phenomenon in 23% of cases.

Table 4. Percentage (P_{ef}) of the IP Classes in Space Weather Effects

Space Weather Effect	Total	ITS	CHS	MIX
GMC	49	62	23	56
Dst	42	63	5	52
Kp	36	60	5	40
Ap	89	93	82	92
PC	28	30	14	40
DB	65	85	36	68
GREE	61	33	82	72
D1	49	42	46	56
*D*2	46	27	60	50
*Z*1	66	50	73	67
*Z*2	51	38	53	58

[27] 2. Strong geomagnetic storms ($Dst < -100$ nT and $Kp > 6.5$) are mostly associated with ITS and MIX classes of the IP sequence. However, the six strongest geomagnetic storms (8% of the SWIT intervals) with maximal $Dst < -200$ nT are caused only by interplanetary transients such as the fast ICME, which are so powerful that they are able to significantly compress and enhance any upstream structure such as the fast solar wind from coronal holes or slow solar wind from interplanetary streamers. Fast solar wind streams and CIRs practically do not contribute to the great geomagnetic storms. This conclusion is in good agreement with results obtained by *Bothmer and Schwenn* [1995].

[28] 3. Strong energy input in the polar cap (*PC* index) is observed in ~28% of the SWIT intervals. The most important drivers of the *PC* index are the ITS and MIX class of events.

[29] 4. *DB* index enhances are observed in 65% of the SWIT intervals. The high *DB* index is generated mostly by the ITS and MIX classes of events. However, CHS events also contribute to the *DB* index in 36% of the cases. Note that the enhancements of the *DB* index are always observed when the *Ap* index is disturbed ($Ap > 20$ nT) or in other words during high long-lasting or extremely strong auroral activity.

[30] 5. Geosynchronous relativistic electron enhancements are observed in 61% of the SWIT events. The main sources of the GREEs are the fast solar wind and MIX events; the ITS class of events produces GREEs only in one third of the cases.

[31] 6. Radiation doses *D*1 and *D*2 on board the Mir station increase in about half of the SWIT intervals. Their enhancements are mostly accompanied with the CHS class of events. However, the ITS and especially MIX events contribute also substantially.

[32] 7. Data failures *Z*1 and *Z*2 on board the Mir station are mostly caused by IP events belonging to both CHS and MIX class events. A contribution of the ITS class of events to the data failures is much smaller.

[33] Here we present two examples of the radiation dose enhancements associated with events from MIX and ITS classes. The MIX event (SWIT-29 interval) on 24–30 September 1998 is presented in Figure 4. Unfortunately the SOHO energetic particle data were not available for this interval. Figure 5 represents the radiation conditions in the outer magnetosphere measured by GOES 8. On the second half of 24 September there was an intense rise in the >10 MeV proton fluxes lasting about 24 hours. The daily dose measurement recorded on board the Mir station was extremely high on this day, suggesting a direct link between the two phenomena. The following day there was a strong geomagnetic storm ($Dst < -200$ nT) accompanied by a long-lasting GMC. These conditions prolonged the high level of the radiation dose, despite the decrease of interplanetary particles observed the previous day. It is interesting to note an enhancement of the radiation dose *D*1 on 29 September, which was accompanied with a GREE during the recovery phase of the recurrent magnetic storm. At the same time on 27 and 29 September the rates of data failures *Z*1 and *Z*2 also increased.

[34] An event from the ITS class (SWIT-18 interval) that occurred on 1–7 May 1998 is presented in Figure 6. An enhancement in the proton spectrum was observed on the 2 May. This enhancement is a magnitude less than what was observed in the previous example (24 September 1998). There is no link between this enhancement (2 May) and the significant increase in the dose *D*1 on board the Mir station that was observed the following day (3 May). On the other hand a long-lasting GMC was encountered on this day and is thought to be the cause of the dose enhancement.

6. Discussion and Summary

[35] Using the SWIT catalogue we have classified solar wind disturbances into three classes of IP sequences: (1) ITS class, associated with interplanetary sheaths (IS) and transients (ICME); (2) CHS class, associated with fast solar wind stream from coronal holes (CH) and corotating interaction regions (CIR); and (3) MIX class, including complex events contributed by IP phenomena from the other two classes. Results of our statistical analysis of the relationship between different classes of IP sequences and space weather effects reflect the basic properties of the solar wind–magnetosphere coupling.

[36] It is well known that radiation dose enhancements are due to SEP events. High-energy and relativistic particles can penetrate from the interplanetary medium to low altitudes and even reach the Earth's surface producing GLEs. The examples presented in Figures 4–6 suggest that only extreme enhancements in the proton spectrum can have a direct influence on low-altitude spacecraft, such as the Mir station. However, phenomena such as ICMEs may cause GMCs and/or strong geomagnetic storms, which may provide the necessary conditions for the penetration of high-energy particles from the interplanetary medium into the region where the low-altitude spacecraft are situated. This is due to the well-known fact that the compression of the dayside magnetosphere causes a decrease in the cutoff energy threshold of the incoming particles. Additionally the ring current formation revealed in *Dst* variation leads to a decrease of the latitude of the trapped radiation boundary [*Tverskaya*, 2000] so that energetic particles from the interplanetary medium can directly penetrate to lower latitudes than during nonstorm conditions.

[37] Strong magnetospheric compression is accompanied with geosynchronous magnetopause crossings, which

Figure 4. Same as Figure 2 but for SWIT-29 interval on 23–30 September 1998. Vertical dashed lines indicate approximate boundaries of the IP structures: interplanetary sheath (IS), interplanetary transient (ICME), and fast solar wind from the coronal holes (CH).

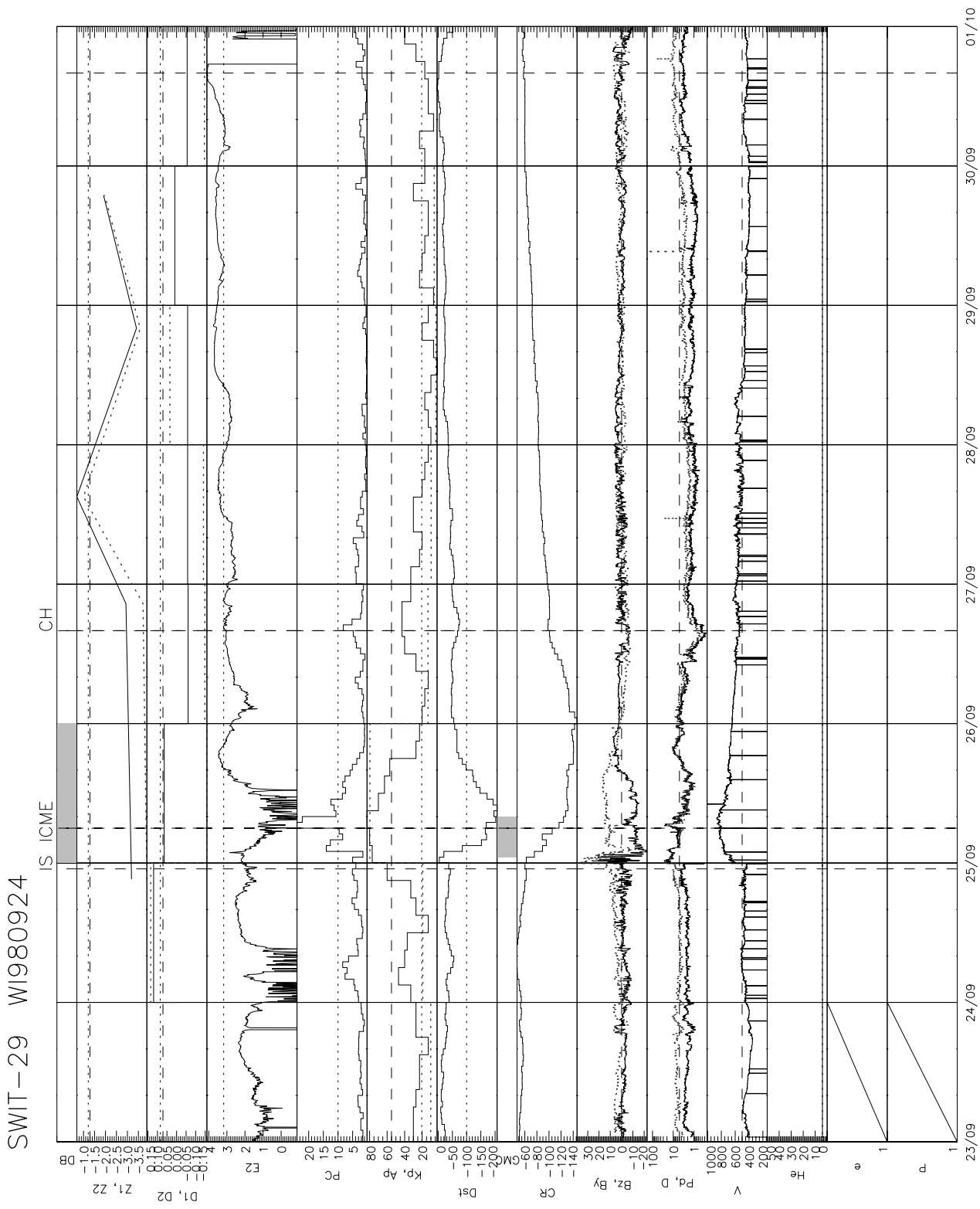
SWIT–29 WI980924
IS ICME
CH
DB
Z1, Z2
D1, D2
F2
PC
Kp, Ap
Dst
GM
CR
Bz, By
Pd, D
V
He
e
p
23/09
24/09
25/09
26/09
27/09
28/09
29/09
30/09
01/10

Figure 4

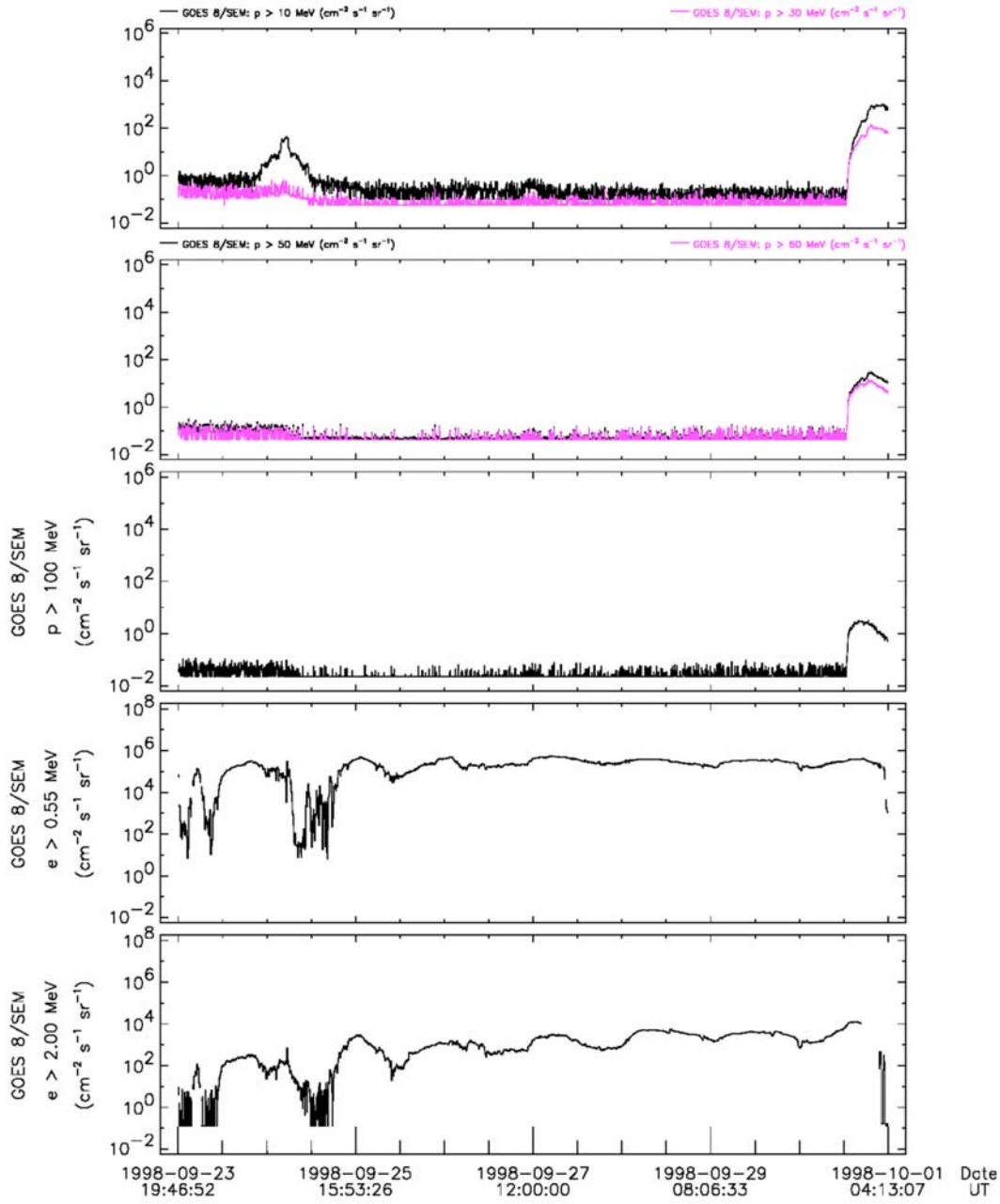

Figure 5. Radiation conditions in the outer magnetosphere measured by GOES 8 on 24–30 September 1998. Top to bottom: time variations of the high-energy proton fluxes (>10 and >30 MeV); fluxes of >50 and >80 MeV protons; flux of >100 MeV protons; time variations of fluxes of >0.55; and time variations of fluxes of >2 MeV electrons.

are associated mostly with the ITS and MIX classes of the IP disturbances. However, we have found that GMCs are often observed in IP events associated with corotating interaction regions (CHS class), where the value of the IMF B_z (about −10 nT) varies very quickly because of compression and Alfven waves, while the moderate dynamic pressure changes gradually. This fact might indicate that the magnetopause response time to the IMF turning southward should be less than the period of the IMF variations in the CIR, which is estimated to

Figure 6. Same as Figure 2 but for SWIT-18 interval on 1–6 May 1998. Vertical dashed lines indicate approximate boundaries of the IP structures: interplanetary sheath (IS) and interplanetary transient (ICME).

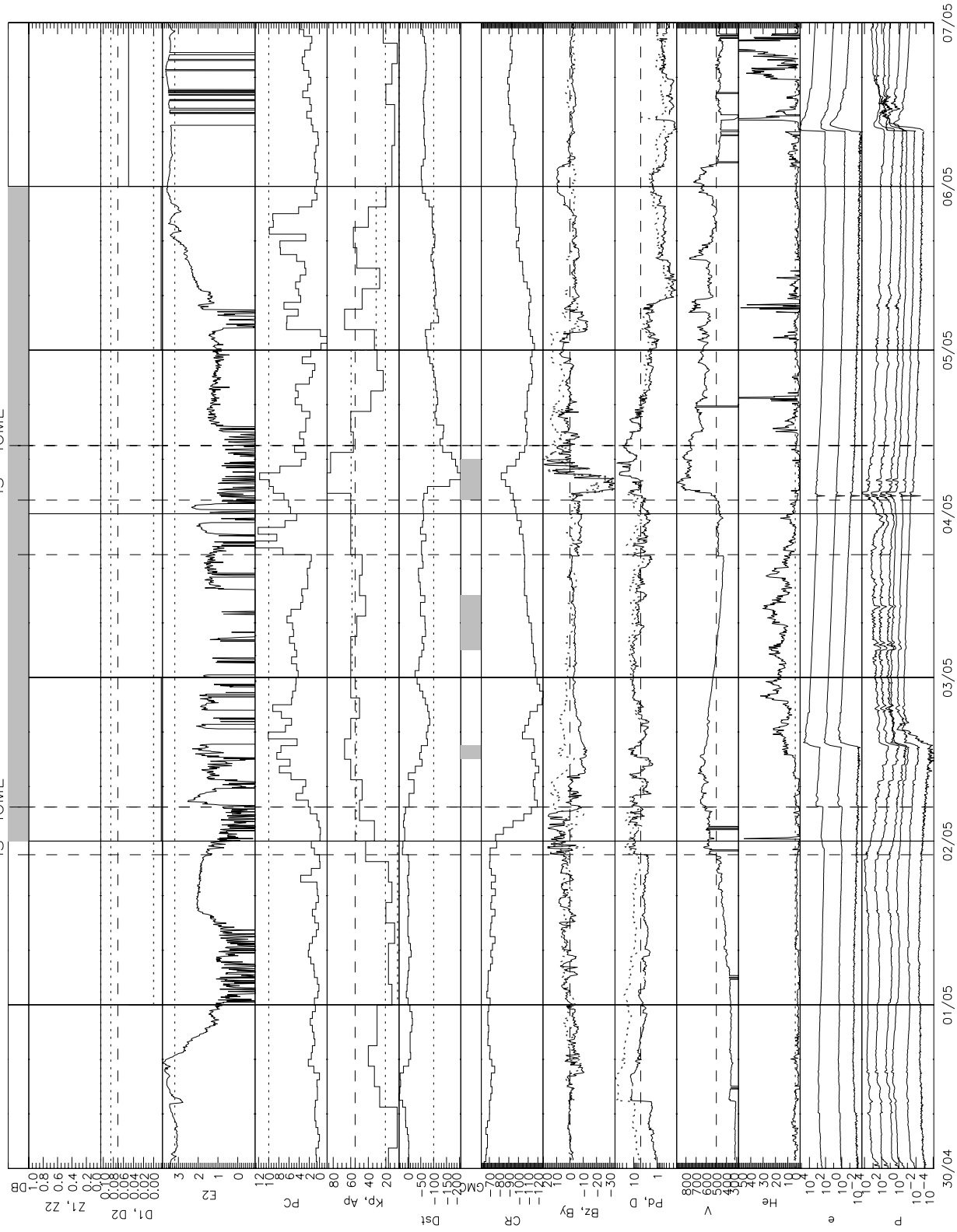
SWIT–18 AC980501
IS ICME
IS ICME
DB
Z1, Z2
D1, D2
E2
PC
Kp, Ap
Dst
GMC
CR
Bz, By
Pd, D
V
He
e
p
30/04
01/05
02/05
03/05
04/05
05/05
06/05
07/05

Figure 6

be about 30 min [*Tsurutani et al.*, 1990]. Otherwise the GMCs should not be observed during CIRs, because the magnetopause would not have enough time to respond to the fast variations of the IMF.

[38] Recently a correlation between the dayside magnetosphere size and relativistic electron fluxes in geosynchronous orbit was found [*Dmitriev and Chao*, 2003]. This fact can explain a weak contribution of the ITS class of events to GREEs. Other parameters controlling the geosynchronous relativistic electron fluxes are solar wind velocity, interplanetary dawn-dusk electric field and *Dst* variation [e.g., *Li et al.*, 2001]. The most significant of these parameters is the solar wind velocity. The physics of this relationship as well as the magnetospheric mechanism responsible for the relativistic electron acceleration is still a subject of debate. It is accepted that the solar wind velocity controls the Kelvin-Helmholtz instability on the magnetopause, which is responsible for Pc4 and Pc5 geomagnetic pulsations [*Miura*, 1992; *Engebretson et al.*, 1998]. The Pc4 and Pc5 pulsations are considered as one of the key processes in the acceleration of relativistic electrons in the outer radiation belt during the geomagnetic storms [*Elkington et al.*, 1999; *Liu et al.*, 1999]. However, *Green and Kivelson* [2001] describe a magnetic storm, for which the Pc4 and Pc5 pulsations are not sufficient to cause a relativistic electron enhancement by themselves. In the discussion of Figure 3 (section 3) we present a case of a fast GREE accompanied with a strong increase in the *PC* index. It is important to note that the solar wind speed in that case was relatively low (<500 km/s). Statistical consideration of the geosynchronous relativistic electron enhancements [*Dmitriev and Chao*, 2003] concludes that a strongly disturbed *PC* index can be regarded as a sufficient condition for the GREE occurrence. The close relationship between the GREEs and the *PC* index indicates a substantial role of the solar wind energy input to the outer magnetosphere in the generation of the relativistic electrons.

[39] On the other hand our statistical analysis of the IP structures shows that the GREEs are mostly associated with the CHS class of IP events, for which the energy input is moderate. Such a contradiction can be resolved by suggesting two mechanisms for relativistic electron acceleration. The first one is fast acceleration during the main phase controlled by high-latitude geomagnetic activity. The second mechanism is long-lasting acceleration operating effectively during the recovery phase of the recurrent magnetic storms, that is controlled by Alfven fluctuations in the fast solar wind streams originating from coronal holes. Note that the latter case is characterized by moderate solar wind pressure and IMF such that the dayside magnetosphere has a nominal size that promotes intensive fluxes of the relativistic electrons in the outer magnetosphere.

[40] The correlation between geosynchronous relativistic electron enhancements and the increase in the data failure rate on board the Mir station is demonstrated in SWIT-24, SWIT-52 and SWIT-29 intervals. The intervals are associated with the fast solar wind intersecting the Earth's magnetosphere (Figures 2, 3, and 4). Moreover, we indicate an increase of the radiation doses on board the Mir station during the main phase of the recurrent magnetic storm on 22–23 July 1998 and during the recovery phase on 24–28 July 1998 (SWIT-24 interval) and on 26–29 September 1998 (SWIT-29 interval) that are accompanied with an increase of the geosynchronous relativistic electron fluxes. A close relationship between enhancements of the data failure rate and radiation doses on board the Mir station with the GREEs is also revealed from the statistical analysis performed above. Indeed space weather effects of *D*1, *D*2, *Z*1, *Z*2 and *GREE* are significantly controlled by the CHS class of the IP sequence.

[41] This fact can be explained by a strong contribution of the relativistic electrons precipitating from the outer radiation belt (ORB) to the radiation environment at low altitudes ($\sim$500 km). It is well known [*Rothwell and McIlwain*, 1960] that the fluxes of relativistic electrons precipitating from the ORB significantly increase during the main phase of geomagnetic storms. The enhancements of the relativistic electrons in the ORB during the recovery phase of recurrent magnetic storms are also accompanied by intensive electron precipitation [*Forbush et al.*, 1962]. The precipitating relativistic electrons penetrate to the low altitudes at middle latitudes where the Mir station spends most of its time during its rotation around the Earth. Therefore during recurrent geomagnetic storms both the equipment and astronauts on board the Mir station are continuously irradiated by strong fluxes of precipitating relativistic electrons. To penetrate through the shielding of the Mir station the electron has to have an energy of more than $\sim$5 MeV [*Dmitriev et al.*, 1998]. Electrons with lower energy generate in the shielding matter the secondary γ radiation that has a high capability for penetration. Hence our results might show that during recurrent geomagnetic storms highly relativistic electron fluxes and/or γ radiation enhance on board the Mir station and can produce an increase of the data failure rate and radiation doses.

[42] Finally we can summarize the results of our statistical study of the radiation conditions on board the Mir station. The relatively high contribution of the IP events from the ITS class to enhancements of the radiation doses can be explained by the fact that during strong geomagnetic storms associated mostly with the ITS class of events the cutoff energy threshold decreases because of compression of the magnetosphere and equatorward shifting of the trapped radiation boundary that provides direct access of the energetic particles from the interplanetary medium to middle latitudes in low-altitude regions. We have showed also the strong association of the failure rates and radiation doses with the CHS class of events that can be attributed to substantial increases in the trapped and precipitating relativistic electron populations in the ORB during recurrent magnetic storms.

[43] **Acknowledgments.** The authors thank NASA/GSFC ISTP for providing data from the Wind, SOHO, ACE, GOES, and LANL

satellites. We thank R. P. Lepping from NASA/GSFC for providing the Wind magnetic data; collaborative efforts of GSFC, UNH, and MIT in providing the Wind plasma data; C. W. Smith from the University of New Hampshire for providing the ACE magnetic data; D. J. McComas from Los Alamos National Laboratory for providing the ACE plasma data; NASA and NOAA for providing the GOES magnetic data; Los Alamos National Laboratory for providing the LANL plasma data; and Kyoto World Data Center for Geomagnetism for providing the *ASY/SYM* indices. This work was supported by grants NSC92-2811-M-008-021, NSC-92-2111-M-008-003, and INTAS 2000-752. N. B Crosby is funded by PRODEX contract 14731. The authors thank Ari Viljanen of the Finnish Meteorological Institute for providing the *DB* index data. The authors thank also the reviewers of this paper for their useful comments and suggestions and Sarah Gibson for proofreading this paper.

References

Akasofu, S.-I. (1981), Energy coupling between the solar wind and the magnetosphere, *Space. Sci. Rev.*, *28*, 121.

Baker, D. N., et al. (1997), Recurrent geomagnetic storms and relativistic electron enhancements in the outer magnetosphere: ISTP coordinated measurements, *J. Geophys. Res.*, *102*, 14,141.

Borrini, G., J. T. Gosling, S. J. Bame, and W. C. Feldman (1982), An analysis of shock wave disturbances observed at 1 AU from 1971 through 1978, *J. Geophys. Res.*, *87*, 4365.

Bothmer, V., and R. Schwenn (1995), The interplanetary and solar causes of major geomagnetic storms, *J. Geomagn. Geoelectr.*, *47*, 1127.

Bothmer, V., I. S. Veselovsky, A. V. Dmitriev, A. N. Zhukov, P. Cargill, E. P. Romashets, and O. S. Yakovchuk (2002), Solar and heliospheric causes of the geomagnetic perturbations during the growth phase of solar cycle 23, *Sol. Syst. Res.*, *36*(6), 498.

Burlaga, L., E. Sittler, F. Mariani, and R. Schwenn (1981), Magnetic loop behind an interplanetary shock: Voyager, Helios, and IMP 8 observations, *J. Geophys. Res.*, *86*, 6673.

Burlaga, L. F., K. W. Behannon, and L. W. Klein (1987), Compound streams, magnetic clouds, and major geomagnetic storms, *J. Geophys. Res.*, *92*, 5752.

Burlaga, L. F., R. M. Skoug, C. W. Smith, D. F. Webb, T. H. Zurbuchen, and A. Reinard (2001), Fast ejecta during the ascending phase of solar cycle 23: ACE observations, 1998–1999, *J. Geophys. Res.*, *106*, 20,957.

Cane, H. V. (2000), Coronal mass ejections and Forbush decreases, *Space Sci. Rev.*, *93*(1–2), 55.

Cane, H. V., and I. G. Richardson (2003), Interplanetary coronal mass ejections in the near-Earth solar wind during 1996–2002, *J. Geophys. Res.*, *108*(A4), 1156, doi:10.1029/2002JA009817.

Cane, H. V., W. C. Erickson, and N. P. Prestage (2002), Solar flares, type III radio bursts, coronal mass ejections, and energetic particles, *J. Geophys. Res.*, *107*(A10), 1315, doi:10.1029/2001JA000320.

Chao, J. K., C. H. Lin, and C. C. Wu (1986), On the propagation and origin of interplanetary shock waves, *Adv. Space Res.*, *6*, 323.

Cohen, C. M. S., R. A. Mewaldt, A. C. Cummings, R. A. Leske, E. C. Stone, P. L. Slocum, M. E. Wiedenbeck, E. R. Christian, and T. T. von Rosenvinge (2001), Forecasting the arrival of shock-accelerated solar energetic particles at Earth, *J. Geophys. Res.*, *106*, 20,979.

Dal Lago, A., W. D. Gonzalez, A. L. C. Degonzalez, and L. E. A. Vieira (2001), Compression of magnetic clouds in interplanetary space and increase in their geoeffectiveness, *J. Atmos. Sol. Terr. Phys.*, *63*(5), 451.

Dmitriev, A. V., and J.-K. Chao (2003), Dependence of geosynchronous relativistic electron enhancements on geomagnetic parameters, *J. Geophys. Res.*, *108*(A11), 1388, doi:10.1029/2002JA009664.

Dmitriev, A. V., and N. B. Crosby (2003), CME influence to the space weather, paper presented at Actual Problems of Solar and Stellar Activity Physics, Russ. Found. for Basic Res., Nizhny Novgorod, Russia, 2–7 June.

Dmitriev, A. V., S. N. Kuznetsov, P. P. Shavrin, V. I. Lyagushin, O. Y. Nechaev, M. I. Panasyuk, E. D. Tolstaya, and M. N. Nikiforova (1998), Distribution of energetic particles and secondary radiation according to orbital station "MIR" data obtained in 1991, *Adv. Space Res.*, *21*, 1797.

Dmitriev, A. V., I. I. Guilfanov, and M. I. Panasyuk (2002), Data failures in the "Riabina-2" experiment on MIR orbital station, *Radiat. Meas.*, *35*, 499.

Elkington, S. R., M. K. Hudson, and A. A. Chan (1999), Acceleration of relativistic electrons via drift-resonant interaction with toroidal-mode Pc-5 ULF oscillations, *Geophys. Res. Lett.*, *26*, 3273.

Engebretson, M., K.-H. Glassmeier, M. Stellmacher, W. J. Hughes, and H. Luhr (1998), The dependence of high-latitude Pc5 wave power on solar wind velocity and on phase of high-speed solar wind streams, *J. Geophys. Res.*, *103*, 26,271.

Forbush, S. E., G. Pizzelia, and D. Venkatesan (1962), The morphology and temporal variations of the Van Allen radiation belt, October 1959 to December 1960, *J. Geophys. Res.*, *67*, 3651.

Gonzalez, W. D., J. A. Joselyn, Y. Kamide, H. W. Kroehl, G. Rostoker, B. T. Tsurutani, and V. M. Vasyliunas (1994), What is a geomagnetic storm?, *J. Geophys. Res.*, *99*, 5771.

Gosling, J. T. (1990), Coronal mass ejections and magnetic flux ropes in interplanetary space, in *Physics of Magnetic Flux Ropes*, *Geophys. Monogr. Ser.*, vol. 58, edited by C. T. Russell, E. R. Priest, and L. C. Lee, p. 343, AGU, Washington, D. C.

Gosling, J. T. (1993), The solar flare myth, *J. Geophys. Res.*, *98*, 18,937.

Gosling, J. T., A. J. Hundhausen, and S. J. Bame (1976), Solar wind stream evolution at large heliocentric distances: Experimental demonstration and the test of a model, *J. Geophys. Res.*, *81*, 2111.

Green, J. C., and M. G. Kivelson (2001), A tail of two theories: How the adiabatic response and ULF waves affect relativistic electrons, *J. Geophys. Res.*, *106*, 25,777.

Hanslmeier, A. (2002), *The Sun and Space Weather*, *Astrophys. Space Sci. Libr.*, vol. *277*, 243 pp., Springer, New York.

Huttunen, K. E. J., H. E. J. Koskinen, and R. Schwenn (2002), Variability of magnetospheric storms driven by different solar wind perturbations, *J. Geophys. Res.*, *107*(A7), 1121, doi:10.1029/2001JA900171.

Kamide, Y., et al. (1998), Current understanding of magnetic storms: Storm-substorm relationship, *J. Geophys. Res.*, *103*, 17,705.

Kudela, K., M. Storini, M. Y. Hofer, and A. Belov (2000), Cosmic rays in relation to space weather, *Space Sci. Rev.*, *93*(1–2), 153.

Li, X., M. Temerin, D. N. Baker, G. D. Reeves, and D. Larson (2001), Quantitative prediction of radiation belt electrons at geostationary orbit based on solar wind measurements, *Geophys. Res. Lett.*, *28*, 1887.

Liu, W. W., G. Rostoker, and D. N. Baker (1999), Internal acceleration of relativistic electrons by large-amplitude ULF pulsations, *J. Geophys. Res.*, *104*, 17,391.

Looper, M. D., J. B. Blake, R. A. Mewaldt, J. R. Cummings, and D. N. Baker (1994), Observations of the remnants of the ultrarelativistic electrons injected by the strong SSC of 24 March 1991, *Geophys. Res. Lett.*, *21*, 2079.

Lühr, H. (1994), The IMAGE magnetometer network, *STEP Int. Newsl.*, *4*(10), 4–6.

Miura, A. (1992), Kelvin-Helmholtz instability at the magnetospheric boundary: Dependence on the magnetosheath sonic Mach number, *J. Geophys. Res.*, *97*, 10,665.

Panasyuk, M. I., M. V. Teltsov, V. I. Shumshurov, and V. V. Tsetlin (1998), Variations of the radiation dose onboard Mir station, *Adv. Space Res.*, *21*, 1635.

Poppe, B. B. (2000), New scales help public, technicians understand space weather, *Eos Trans. AGU*, *81*(29), 322.

Rothwell, P., and C. McIlwain (1960), Magnetic storms and the Van Allen radiation belts: Observations from satellite 1958ε (Explorer IV), *J. Geophys. Res.*, *65*, 799.

Sheeley, N. R., R. A. Howard, M. J. Koomen, D. J. Michels, R. Schwenn, K. H. Mahlhauser, and H. Rosenbauer (1985), Coronal mass ejections and interplanetary shocks, *J. Geophys. Res.*, *90*, 163.

Suvorova, A. V., A. Dmitriev, J.-K. Chao, M. Thomsen, and Y.-H. Yang (2005), Necessary conditions for geosynchronous magnetopause crossings, *J. Geophys. Res.*, *110*, A01206, doi:10.1029/2003JA010079.

Troshichev, O. A., V. G. Andersen, S. Vennerstorm, and E. Friis-Christensen (1988), Magnetic activity in the polar cap—A new index, *Planet. Space Sci.*, *36*, 1095.

Tsurutani, B. T., and W. D. Gonzalez (1987), The cause of high-intensity long-duration continuous *AE* activity (HILDCAAS): Interplanetary Alfven wave trains, *Planet. Space. Sci.*, *35*, 405.

Tsurutani, B. T., T. Gould, B. E. Goldstein, W. D. Gonzalez, and M. Sugiura (1990), Interplanetary Alfven waves and auroral (substorm) activity: IMP 8, *J. Geophys. Res.*, *95*, 2241.

Tsurutani, B. T., W. D. Gonzalez, A. L. C. Gonzalez, F. Tang, J. K. Arballo, and M. Okada (1995), Interplanetary origin of geomagnetic activity in the declining phase of the solar cycle, *J. Geophys. Res.*, *100*, 21,717.

Tverskaya, L. V. (2000), Diagnosing the magnetospheric plasma structures using relativistic electron data, *Phys. Chem. Earth*, *25*(1–2), 39.

Tverskaya, L. V., M. I. Panasyuk, S. Y. Reizman, E. N. Sosnovets, M. V. Teltsov, and V. V. Tsetlin (2004), The features of radiation dose variations onboard ISS and Mir space station: Comparative study, *Adv. Space Res.*, *34*, 1424.

Tylka, A. J. (2001), New insight on solar energetic particles from Wind and ACE, *J. Geophys. Res.*, *106*, 22,333.

Wilcox, J. M., and N. F. Ness (1965), Quasi-stationary corotating structure in the interplanetary medium, *J. Geophys. Res.*, *70*, 1815.

Zhang, J., J. Woch, S. K. Solanki, R. von Steiger, and R. Forsyth (2003a), Interplanetary and solar surface properties of coronal holes observed during solar maximum, *J. Geophys. Res.*, *108*(A4), 1144, doi:10.1029/2002JA009538.

Zhang, J., K. P. Dere, R. A. Howard, and V. Bothmer (2003b), Identification of solar sources of major geomagnetic storms between 1996 and 2000, *Astrophys. J.*, *582*, 520.

J.-K. Chao and A. V. Dmitriev, Institute of Space Science, National Central University, Chung-Li, Taoyuan 320, Taiwan. (jkchao@jupiter.ss.ncu.edu.tw; dalex@jupiter.ss.ncu.edu.tw)

N. B. Crosby, Belgian Institute for Space Aeronomy, Ringlaan-3-Avenue Circulaire, B-1180 Brussels, Belgium. (norma.crosby@oma.be)